



Couple effect of surface energy and strain gradient on the mechanical behaviors of the biological staggered composites



Yanwei Liu^a, Hansong Ma^b, Hao Long^a, Yueguang Wei^{a,*}

^a Department of Mechanics and Engineering Science, College of Engineering, BIC-ESAT, Peking University, Beijing 100871, PR China

^b State-Key Laboratory of Nonlinear Mechanics, Institute of Mechanics, Chinese Academy of Sciences, Beijing 100190, PR China

ARTICLE INFO

Keywords:

Biological staggered composites
Strain gradient
Surface energy
Trans-scale shear-lag model
Size effect

ABSTRACT

Biological staggered composites, which are hierarchy spanning from nano scale to macro scale, boast remarkable mechanical properties. In this paper, a trans-scale shear-lag model is established based on the strain gradient theory and the Gurtin-Murdoch model, which provides a chance to glimpse how the micro-nano structures of the biological composite determine its macroscopic mechanical behavior. With the trans-scale shear-lag model, we found that the deformation, stress distribution and overall effective modulus have strong size effects, which are related to the thickness of the ‘matrix’ and ‘platelet’ of the biological staggered composites. Based on the analysis, two normalized numbers d/l and $E_s/(hE_p)$ are proposed to describe the size effects caused by the thickness of the matrix and platelet, respectively. Besides, the predicted effective moduli of the biological staggered structure composites are compared with the experiments to verify our trans-scale shear-lag model. Our research sheds light on the understanding of the mechanical behaviors of the staggered biological composites and provides theoretical guidance for the design of high-performance bionic composite materials.

1. Introduction

Nature has produced many materials with excellent performance, such as bone, teeth, shell and antler, during thousands of years of evolution. These biological materials are made up of mineral as brittle as chalk and protein as soft as skin, but exhibit a perfect combination of toughness and stiffness compared to their constituents. For example, the shell is composed of 1 ~ 5% vol. protein and 95 ~ 99% vol. mineral. Its modulus is about 50 GPa, which can be comparable to that of mineral (50 ~ 100 GPa), and its strength is 100 ~ 300 MPa, which is 3 ~ 10 times that of the mineral; besides, the fracture toughness of the shell (3 ~ 7 MPa m^{1/2}) is also greater than that of mineral (□1 MPa m^{1/2}) [1–4] and comparable to that of skin [5]. Similarly, the bone, made up of 55 ~ 60% vol. collagen and 40 ~ 45% vol. mineral, also possesses excellent mechanical properties. Its strength and fracture toughness are higher than those of the mineral, and its modulus is comparable to that of the mineral [6,7]. These remarkable mechanical properties of biological composites attract extensive attention from researchers with the objective of imitating nature to manufacture high-performance bionic composite materials.

The combination of toughness and stiffness of the biological composites is attributed to the hierarchy bottom up from nanoscale

[2,4,8–11]. For example, there are three-layer structures in seashell (periostracum layer, prismatic layer and nacreous layer) [2,4,10,11] and more than seven hierarchical levels in bone [9,12]. Despite their complex structures, the basic building block in biological composites is the staggered structure at the micro-nano scale [8]. For example, the nacre occupying the majority of the volume of shell is a “brick and mortar” structure, where the thickness of the staggered platelets is 0.2 ~ 1 μm and that of the matrix gluing the platelets together is 20 ~ 40 nm [13,14]; the mineralized fibril in bone consists of mineral platelets with a thickness of a few nanometers (~2 nm) staggered in a collagen matrix [12]. This staggered structure at the micro-nano scale is found to be a main factor contributing to the large stiffness of biological composites [8]. In order to better design the artificial composites, the mechanical model for the relationship between the staggered structure at the micro-nano scale and the overall effective modulus has been investigated for many years. In the early stage, researchers mainly focused on the relationship between the staggered structure and the overall effective modulus [7,8,15–20]. For example, Jäger and Fratzl [7] proposed a model with a staggered array of platelets for the collagen fibrils and explored the dependence of the mechanical behaviors on the geometric features of the platelet and matrix. Inspired by the work of Jäger and Fratzl, Ji and Gao [8] developed a

* Corresponding author.

E-mail address: weiyg@pku.edu.cn (Y. Wei).

tension-shear-chain model (TSC model), where they assumed the shear stress between the platelet and the matrix is uniform, to predict the mechanical properties of the staggered composites, and they pointed out that the large stiffness of biological materials is attributed to the large aspect ratio and staggered structure. After that, with the consideration of the non-uniform shear stress between the platelet and the matrix, Zuo and Wei [18] improved the TSC model and established a shear-lag model (SL model). Then, SL model was used by Gao [21] to study the mechanical properties of hierarchical materials and the results show that the non-uniform shear stress between the platelet and the matrix cannot be neglected when the number of the hierarchy is large. Both TSC model and SL model are based on the assumption that the mineral platelets in the staggered structure only bear the tensile stress, while the organic layers only bear the shear stress. Based on the SL model also, Bar-on and Wagner [19] established a general mechanical model (BW model) that considered both the tensile and shear deformation in the mineral platelet and organic matrix. Besides, the effects of the arbitrary distribution of the unidirectional platelets and the waviness of the platelet on the mechanical properties of the staggered composites were also widely studied by previous researchers [16,17,20].

With the improvement of the understanding of the mechanical behaviors of materials at the micro-nano scale, researchers further pay attention to the scale characteristics on the basis of focusing on the staggered structure. Many studies have shown that the higher-order continuum theory (e.g. strain gradient theory) can describe the mechanical behaviors of materials at the micron scale due to its ability that captures microstructure effects resulting from non-local interactions of material particles [22–27]. This theory is applicable to both a continuum medium with microstructure and a non-local medium including long-range interactions. Based on the strain gradient theory, Ma et al. [24] extended SL model and derived a strain gradient shear-lag model. They systematically studied the size effect of the mechanical behaviors of biological staggered composites and found that the size effect depends on the thickness of the organic matrix layer, and the thinner the thickness of the organic matrix layer, the stiffer the staggered structure materials. Different from the work of Ma et al. [24], other researchers consider the effect of the surface energy on the mechanical behaviors of staggered structure composites. The surface elasticity theory developed by Gurtin and Murdoch [28] can reflect the surface energy arising from the difference of arrangements between the surface atom and the inner atom [28], which has been widely considered in the mechanical characterization of nanostructure and has been proved to be effective [28–33]. Based on the Gurtin-Murdoch model, Dong et al. [34] introduced the surface effect into the TSC model and analyzed the influence of the interface effect on the effective modulus of biological staggered composites. The results show that the size effect of the mechanical properties of biological staggered composites is related to the thickness of the mineral platelet. From the researches of Ma et al. [24] and Dong et al. [34], it can be found that the influence of scale characteristics on the biological staggered composite is significant. However, for the biological staggered composites made of mineral platelets and organic materials, the size effect should depend on both the scale characteristic of the mineral platelet and that of the organic matrix layer, but not on the scale characteristic of one of them. Up to now, a model which can reflect both the scale characteristic of the mineral platelet and that of the organic matrix layer has not been proposed. Moreover, it is also not clear how the scale characteristic of the mineral platelet and that of the organic matrix layer are coupled to influence the mechanical behaviors of staggered structure materials. Therefore, in order to design bionic composite materials with high strength and toughness, a general model that can reflect the staggered structure characteristic and the scale characteristic of mineral platelets and organic matrix needs to be put forward.

Considering the problems in current researches, in this paper, we establish a trans-scale shear-lag mechanical model that includes the scale and staggered structure characteristics of biological staggered composites based on the strain gradient theory and the Gurtin-Murdoch model. What should be emphasized is that our model can simultaneously describe the size effects caused by the organic layer and the mineral platelet, and provides a chance to glimpse that how the microstructure of the biological composite influences its macroscopic mechanical behaviors. The paper is organized as follows: In Section 2, firstly, the simplified strain gradient theory developed by Wei and Hutchinson [35] and the Gurtin-Murdoch surface elasticity theory [28] are reviewed; then, the trans-scale shear-lag model is introduced in detail. In Section 3, with the model, the size effects caused by the thickness of mineral platelet and organic layer are analyzed from three aspects: the deformation state, the stress distribution and the overall effective modulus of the biological staggered composites. The effective moduli predicted by the trans-scale shear-lag model are compared with the experiment results to verify our model in Section 4. In Section 5, the main conclusions are summarized. Our research sheds light on the understanding of the size effect of the mechanical behaviors of biological staggered composites and provides theoretical guidance for the design of the bionic composite materials with high strength and toughness.

2. Theory and model

The strain gradient and surface energy play important roles in the mechanical behaviors of structures at the micro-nano scale. In order to establish a general trans-scale model for the biological staggered composites, firstly, the simplified strain gradient theory developed by Wei and Hutchinson and the Gurtin-Murdoch surface elasticity theory are reviewed. Then the detailed processes of the model establishment are introduced. Finally, based on our trans-scale model, the size effect characteristic of the mechanical behaviors of biological staggered composites is analyzed.

2.1. The simplified strain gradient theory

The strain gradient theory developed by Wei and Hutchinson based on Mindlin [25] with five constants is one with just three constants containing two Lamé constants and one characteristic length [36]. The constitutive equations and geometrical equations for this simplified gradient theory are

$$\sigma_{ij} = \lambda \varepsilon_{kk} \delta_{ij} + 2\mu \varepsilon_{ij} \quad \tau_{ijk} = 2El^2 \kappa_{ijk} \quad (1)$$

$$\varepsilon_{ij} = \frac{1}{2}(u_{i,j} + u_{j,i}) \quad \kappa_{ijk} = \partial_i \partial_j u_k = u_{k,ij} = u_{k,ji} \quad (2)$$

where σ_{ij} and τ_{ijk} are the stress and high-order stress tensor; ε_{ij} and κ_{ijk} are the strain and high-order strain tensor; u_i is the displacement vector; the comma stands for derivation; λ and μ are the classical Lamé constants; E is Young's modulus; δ_{ij} is Kronecker delta; l is the characteristic length of material; Latin indices (i, j and k) run from 1 to 3. It should be noted that we adopt a simplified strain gradient constitutive equation for convenience, and the general strain gradient constitutive equation can be found in previous researches [25,37]. The variation of the strain energy is

$$\delta W = \int_V \sigma_{ij} \delta \varepsilon_{ij} + \tau_{ijk} \delta \kappa_{ijk} dV \quad (3)$$

When the surface of the solid is smooth, based on Stokes' theorem and Gauss' flux theorem, Eq. (3) can be expressed as

$$\delta W = \int_V \tau_{ijk,ij} \delta u_k - \sigma_{kij} \delta u_k dV + \int_{\partial V} \sigma_{ij} n_j \delta u_i - \tau_{ijk,j} n_i \delta u_k + (D_i n_i) n_j n_i \tau_{ijk} \delta u_k - D_i (n_j \tau_{ijk}) \delta u_k dS + \int_{\partial V} \tau_{ijk} n_i n_j D \delta u_k dS \quad (4)$$

where $D_j \equiv (\delta_{jk} - n_j n_k) \partial_k$, $D \equiv n_i \partial_i$; n_i is the normal vector of the surface. What needs to be emphasized is that if the surface has an edge, there will be an edge force [25,38]. Eq. (4) suggests that the variation of work done by external forces is

$$\delta W_1 = \int_V f_k \delta u_k dV + \int_{\partial V} t_k \delta u_k dS + \int_{\partial V} r_k (D \delta u_k) dS \quad (5)$$

where f_k is the body force; t_k is the surface traction; r_k is the double stress traction. From Eqs. (4) and (5), the equilibrium equation reads

$$\sigma_{ik,i} - \tau_{ijk,ij} + f_k = 0 \quad (6)$$

and the boundary conditions are

$$t_k = \sigma_{ki} n_i - \tau_{ijk,j} n_i + (D_i n_i) n_j n_i \tau_{ijk} - D_i (n_j \tau_{ijk}) \quad (7a)$$

$$r_k = n_i n_j \tau_{ijk} \quad (7b)$$

2.2. The Gurtin-Murdoch model

The surface elasticity developed by Gurtin and Murdoch abstracted the surface as a mathematical surface without thickness, and the constitutive equation and the geometrical equation of the surface can be expressed as [39]

$$\tau_{\alpha\beta}^s = C_{\alpha\beta\gamma\eta}^s \cdot \varepsilon_{\gamma\eta}^s \quad (8a)$$

$$\varepsilon_{\gamma\eta}^s = \frac{1}{2} (u_{\gamma,\eta}^s + u_{\eta,\gamma}^s) \quad (8b)$$

where $\tau_{\alpha\beta}^s$ is the surface stress tensor; $C_{\alpha\beta\gamma\eta}^s$ is the surface stiffness tensor; u^s is the displacement vector of the surface; $\varepsilon_{\alpha\beta}^s$ is the surface strain tensor. α, β, γ and η run from 1 to 2. Recently, a simplified surface elasticity theory is developed by Rosi et al., which can be found in reference [40]; here, we will not go into the details about it. Based on the generalized Young-Laplace equation, the equilibrium equations on the normal direction and the tangential direction of the surface [39,41] are

$$\Delta \sigma_{ij} n_i n_j = -\tau_{\alpha\beta}^s \kappa_{\alpha\beta}^s \quad (9a)$$

$$P_{mi} \Delta \sigma_{ij} n_j = -\tau_{\alpha\beta}^s \alpha_{\alpha\beta} \quad (9b)$$

where $P_{mi} = \delta_{mi} - n_m n_i$; $\Delta \sigma_{ij} = \sigma_{ij}^{(2)} - \sigma_{ij}^{(1)}$ represents the stress difference across the interface; $\tau_{\alpha\beta}^s$ is the stress on the interface; $\kappa_{\alpha\beta}^s$ denotes the curvature of the surface. Moreover, Eq. (9) can also be understood as the governing equation of stress transmission across the interface. For the perfect interface, the displacement of the surface is consistent with that of the block material:

$$u^s = u^{(1)}|_{x,y,z = surface} = u^{(2)}|_{x,y,z = surface} \quad (10)$$

For the one-dimensional interface without curvature as shown in Fig. 1, based on Eq. (8), it can be known

$$\tau^s = E^s u_{1,1}^s \quad (11)$$

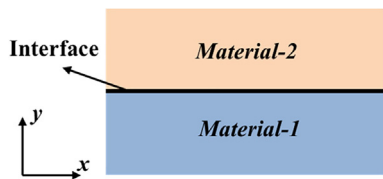


Fig. 1. The diagram of a one-dimensional interface without curvature.

Following Eqs. (9) and (10), the stress transmission across the interface and the displacement of the surface read

$$\sigma_{22}^{(2)} - \sigma_{22}^{(1)} = 0 \quad (12a)$$

$$\sigma_{21}^{(2)} - \sigma_{21}^{(1)} = -\frac{d\tau^s}{dx} \quad (12b)$$

$$u^s = u^{(1)}|_{y = surface} = u^{(2)}|_{y = surface} \quad (13)$$

2.3. The general trans-scale shear-lag model for the biological staggered composites

The diagram of the biological staggered composite is shown in Fig. 2(a). The foundation assumptions for the establishment of the trans-scale shear-lag model are

(a) Because the modulus ratio of the mineral platelet to the organic matrix is more than 10^3 and the aspect ratio of the mineral platelet is large, we assume that the tensile force is mainly carried by the mineral platelet and the shear force is mainly born by the organic matrix. In addition, the organic matrix between the end of the mineral platelet is far shorter than the length of the mineral platelet, and consequently, the load carried by the organic matrix in this area is neglected. Therefore, when a tensile load F is applied on the biological staggered composite, the transmission path of force is shown in Fig. 2(b). At this time, the volume ratio of the mineral platelet to the organic matrix approximately equals the thickness ratio of them h/d ;

(b) Based on the assumptions in (a), we can say that there are only tensile deformation in the mineral platelet and shear deformation in the organic matrix, and the tensile deformation of the mineral platelet is uniform along y and varies along x. Namely, u_p is a function of x. In addition, the shear deformation of the organic matrix occupies the majority of the deformation of the staggered structure, and the aspect ratio of the platelet is large. Therefore, the strain gradient effect in the platelet can be neglected. Namely, the platelet is regarded as a traditional elastic material;

(c) Because the thickness of the organic matrix is much smaller than its length. At this time, the derivative of the displacement of organic matrix to y is much larger than that to x. So only the strain gradient effect in the organic matrix along y is considered.

Considering the periodicity of the staggered structure composites, a representative cell is extracted as shown in Fig. 2(c), and the equilibrium analysis of its infinitesimal elements is shown in Fig. 3 based on assumptions (a), (b) and (c).

For the mineral platelet, the moments caused by the surface traction and double-stress traction are balanced by the other half platelet. According to the equilibrium analysis, the balance equations for the platelets and organic matrix without body force are

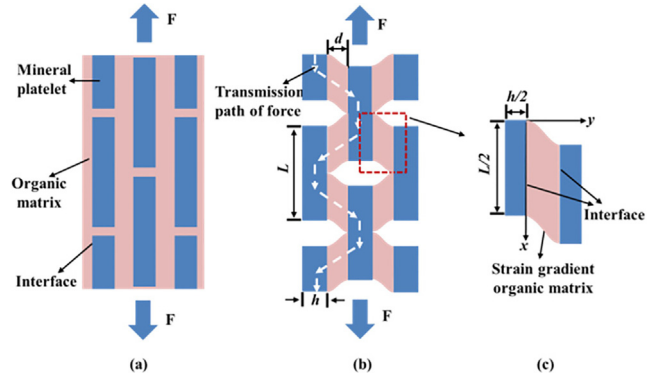


Fig. 2. (a) The diagram of biological staggered composite; (b) The transmission path of force in the composite; (c) Representative cell of the composite.

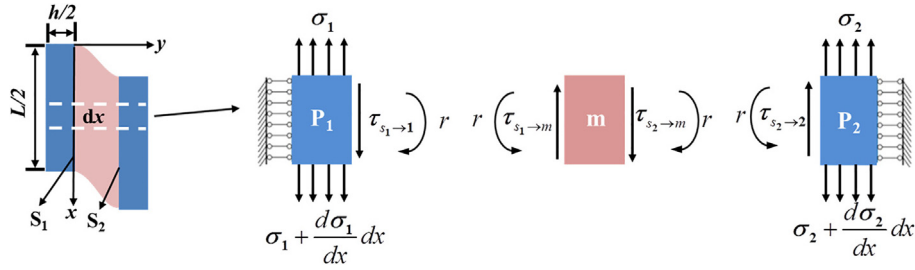


Fig. 3. The equilibrium analysis of the infinitesimal elements of the staggered structure composites.

$$\frac{d\sigma_1}{dx} \times \frac{h}{2} + \tau_{s_1 \rightarrow 1} = 0 \quad (14a)$$

$$\tau_{s_1 \rightarrow m} = \tau_{s_2 \rightarrow m} = t \quad (14b)$$

$$\frac{d\sigma_2}{dx} \times \frac{h}{2} - \tau_{s_2 \rightarrow 2} = 0 \quad (14c)$$

where σ_1 and σ_2 are the tensile stress on the mineral platelets P_1 and P_2 , respectively. $\tau_{s_1 \rightarrow 1}$ is the shear stress of the interface S_1 on the mineral platelet P_1 ; $\tau_{s_2 \rightarrow 2}$ is the shear stress of the interface S_2 on the mineral platelet P_2 ; $\tau_{s_1 \rightarrow m}$ and $\tau_{s_2 \rightarrow m}$ are the interfaces S_1 and S_2 on the organic matrix. Following Eq. (12), it can be known that

$$\tau_{s_1 \rightarrow m} - \tau_{s_1 \rightarrow 1} = -\frac{d\tau^{s_1}}{dx} \quad (15a)$$

$$\tau_{s_2 \rightarrow 2} - \tau_{s_2 \rightarrow m} = -\frac{d\tau^{s_2}}{dx} \quad (15b)$$

where τ^{s_1} and τ^{s_2} are the surface stress of the interfaces S_1 and S_2 , respectively. Based on Eqs. (1), (2), (7a) and (11), the stresses expressed by displacement read

$$t = n_2(\sigma_{21} - \partial_2 \tau_{221}) = G_m \frac{\partial u_m}{\partial y} - 2El^2 \frac{\partial^3 u_m}{\partial y^3} \quad (16a)$$

$$\sigma_1 = E_p \frac{du_{p1}}{dx} \quad \sigma_2 = E_p \frac{du_{p2}}{dx} \quad (16b)$$

$$\tau^{s_1} = E^s \frac{du^{s_1}}{dx} \quad \tau^{s_2} = E^s \frac{du^{s_2}}{dx} \quad (16c)$$

where G_m is the shear modulus of the organic matrix. u_{p1} and u_{p2} are the displacements of platelets P_1 and P_2 along x , respectively. u_m is the displacement of the organic matrix. u^{s_1} and u^{s_2} are the displacements of surfaces S_1 and S_2 , respectively. Using Eqs. (15) and (16) in Eq. (14), we can get the governing equations for this problem:

$$\frac{E_p h}{2} \frac{d^2 u_{p1}}{dx^2} + E^s \frac{d^2 u^{s_1}}{dx^2} + t = 0 \quad (17a)$$

$$t = G_m \frac{\partial u_m}{\partial y} - 2El^2 \frac{\partial^3 u_m}{\partial y^3} \quad (17b)$$

$$\frac{E_p h}{2} \frac{d^2 u_{p2}}{dx^2} + E^s \frac{d^2 u^{s_2}}{dx^2} - t = 0 \quad (17c)$$

The boundary conditions are

$$\begin{aligned} u_{p1}|_{x=0} &= 0; \quad \sigma_2|_{x=0} = 0 \\ \sigma_1|_{x=L/2} &= 0; \quad \sigma_2|_{x=L/2} = \sigma_{max} \end{aligned} \quad (18)$$

We assume that the interfaces S_1 and S_2 are perfect, and the displacement and its normal gradient Du_i is continuous. Then the continuous conditions are

$$u_m|_{y=0} = u_{p1} = u^{s_1}; \quad Du_m|_{y=0} = Du_{p1}|_{y=0} = Du^{s_1} = 0 \quad (19a)$$

$$u_m|_{y=d} = u_{p2} = u^{s_2}; \quad Du_m|_{y=d} = Du_{p2}|_{y=d} = Du^{s_2} = 0 \quad (19b)$$

Based on the governing equations, the boundary conditions and the continuous conditions, the problem can be solved as follows: using Eq. (19) in Eq. (17b), we obtain

$$u_m = \frac{\begin{pmatrix} u_{p2} e^{A d} - u_{p2} e^{A(d+y)} - u_{p1} e^{A d} - u_{p1} e^{A(d+y)} + u_{p1} e^{A y} \\ + u_{p2} e^{A y} + u_{p1} e^{2A y} - u_{p2} e^{2A y} - A u_{p1} y e^{A y} + A u_{p2} y e^{A y} \\ + A d u_{p1} e^{A(d+y)} - A u_{p1} y e^{A(d+y)} + A u_{p2} y e^{A(d+y)} + A d u_{p1} e^{A y} \end{pmatrix}}{2e^{A y} - 2e^{A(d+y)} + A d e^{A(d+y)} + A d e^{A y}} \quad (20a)$$

$$t = -\frac{A(u_{p1} - u_{p2}) \left(G_m e^{A y} - G_m e^{A d} - G_m e^{2A y} + G_m e^{A(d+y)} \right)}{2e^{A y} - 2e^{A(d+y)} + A d e^{A(d+y)} + A d e^{A y}} \quad (20b)$$

where $A = \sqrt{\frac{G_m}{2E_m l^2}}$. l is the characteristic length of the organic matrix. By Eqs. (17a), (17c), (18) and (20), the displacements of the mineral platelets are

$$u_{p1} = C_1 + C_2 x - C_3 e^{Bx} - C_4 e^{-Bx} \quad (21a)$$

$$u_{p2} = C_1 + C_2 x + C_3 e^{Bx} + C_4 e^{-Bx} \quad (21b)$$

where

$$B = \sqrt{\frac{2n}{K}}; \quad K = \frac{E_p h}{2} + E^s; \quad n = \frac{G_m}{d[1 - \frac{2(e^{Ad}-1)}{Ad(e^{Ad}+1)}]} \quad (22a)$$

$$\begin{aligned} C_1 &= -\frac{\frac{\sigma_{max}}{E_p} + \frac{\sigma_{max}}{E_p} e^{\frac{B}{2} l}}{2(B - B e^{\frac{B}{2} l})}; \quad C_2 = \frac{\sigma_{max}}{2}; \quad C_3 = -\frac{\frac{\sigma_{max}}{E_p}}{2(B - B e^{\frac{B}{2} l})}; \quad C_4 \\ &= -\frac{\frac{\sigma_{max}}{E_p} e^{\frac{B}{2} l}}{2(B - B e^{\frac{B}{2} l})} \end{aligned} \quad (22b)$$

Based on Eq. (16b), the tensile stresses in the mineral platelets are

$$\sigma_1(x) = E_p(C_2 - C_3 B e^{Bx} + C_4 B e^{-Bx}) \quad (23a)$$

$$\sigma_2(x) = E_p(C_2 + C_3 B e^{Bx} - C_4 B e^{-Bx}) \quad (23b)$$

The overall effective modulus of the biological staggered composites is defined as the ratio of the effective stress to the effective strain. Then the compact form of the effective modulus can be written as

$$\frac{1}{E_c} = \frac{\varepsilon}{\sigma} = \frac{\left(\frac{u_{p2}(L/2) - u_{p1}(0)}{L/2} \right)}{\left(\frac{\sigma_{max} \times \frac{h}{2}}{h+d} \right)} = \frac{1}{\phi E_p} + \frac{4}{\eta \phi E_p \tanh\left(\frac{\eta}{4}\right)} \quad (24)$$

where $\eta = \frac{\eta_c}{\sqrt{1 - \frac{2(e^{Ad}-1)}{Ad(e^{Ad}+1)}}}$; $\eta_c = 2\rho \sqrt{\frac{G_m h}{E_p(\frac{2E_s}{E_p} + 1)d^2}}$; $\rho = L/h$; $\phi = \frac{h}{d+h}$.

From Eq. (24), it can be known that the mechanical size effect of the staggered composites depends on two dimensionless numbers d/l and $E_s/(E_p h)$. $E_s/(E_p h)$ and d/l reflect the size effects due to the mineral

platelet and the organic matrix, respectively. When E_s and E_p are constants, the smaller the thickness of the mineral platelet, the larger the value of $E_s/(E_p h)$. At this time, the size effect caused by the mineral platelet becomes stronger. If the surface effect is neglected ($E_s = 0$), our solution is reduced to the SGSL model [24]. When the thickness of the organic matrix, d , is far smaller than its characteristic length, l , $1 - [2(e^{Ad} - 1)]/[Ad(1 + e^{Ad})]$ tends to zero. At this time, the effective modulus E_c tends to infinity based on Eq. (24). Namely, the size effect due to the thickness change of the organic matrix is very strong. When d is much larger than l , d/l tends to infinity. At this time, $1 - [2(e^{Ad} - 1)]/[Ad(1 + e^{Ad})]$ tends to 1, and then our model that has ignored the surface effect will be further reduced to the traditional SL model [18]. Based on the above analysis, it can be found that by considering the influences of the strain gradient and surface energy, our model can reflect both the size effect caused by the mineral platelet and that caused by the organic matrix. In other words, our model constructs a bridge between the micro-nano structure of biological staggered composite and its macroscopic mechanical behavior.

3. Results and discussion

In this section, the size effects caused by the thickness change of the mineral platelet and the organic matrix on the mechanical behaviors of the staggered structure composites are investigated based on the solution of displacement, stress, and effective modulus given by the proposed model. Because the thickness of the organic matrix is usually several nanometers to tens of nanometers [12,13] and the length scale, l , is about several micrometers [24,42], d/l is taken to be 0.01 ~ 100 in the following results to cover the possible range in reality. In addition, the thickness of the mineral platelet is always several nanometers to several micrometers [12,13], and the modulus of the mineral platelet is 50 ~ 100 GPa [8], so we take $E_s/(E_p h)$ as $-0.4 \sim 0.4$ according to the value of E_s taken by other researches [29,34]. Here, we mainly focus on the effects of the strain gradient and surface energy on the mechanical behaviors of the biological staggered composites. Therefore, with regard to other parameters, such as E_m/E_p , ϕ , and ρ , a common set of values are selected [24].

3.1. Size effect of the deformation and tensile stress in the mineral platelet

Since the mineral platelets P_1 and P_2 are antisymmetric, only the displacements and stresses distributions of the mineral platelet P_1 are analyzed. Based on the dimensionless analysis, we can know that the normalized displacement of the mineral platelet P_1 , $u_{p1}/(\sigma_{max}L/E_p)$, is a function of $E_s/(E_p h)$, E_m/E_p , ϕ , ρ , β and x/L from Eq. (21a): $u_{p1}/(\sigma_{max}L/E_p) = f(E_s/(E_p h), E_m/E_p, \phi, \rho, \beta, x/L)$. Fig. 4 shows the dis-

placement of the mineral platelet P_1 along x at different β and $E_s/(E_p h)$. From Fig. 4(a), it can be known that $u_{p1}/(\sigma_{max}L/E_p)$ increases with the increase of x/L , but the increasing pattern is different under different β . In classical case ($\beta = \infty$), the relationship between $u_{p1}/(\sigma_{max}L/E_p)$ and x/L is parabolic, which denotes the deformation at different points is non-uniform and the strain decreases gradually with the increase of x/L . The relationship between $u_{p1}/(\sigma_{max}L/E_p)$ and x/L becomes more and more linear along with the decrease of β , which represents the deformation at different points is more uniform than before. In addition, surprisingly, there is little difference in the total tensile deformation of the mineral platelet at different β (the total deformation, $u_{p1}/(\sigma_{max}L/E_p)|_{x=0.5} - u_{p1}/(\sigma_{max}L/E_p)|_{x=0}$, is always 0.25 at different β). In other words, the size effect due to the decrease of the organic matrix thickness only influences the deformation pattern of the mineral platelet but has no significant effects on its total tensile deformation. Similar to the above case, the size effect due to the decrease of the platelet thickness also only changes the deformation pattern of the platelet and does not affect its total deformation, which is shown in Fig. 4 (b). For example, with the decrease of the surface modulus, the relationship between $u_{p1}/(\sigma_{max}L/E_p)$ and x/L becomes more and more linear, and the total tensile deformation of the platelet has no change. From the above analysis, it can be found that the strain gradient and the surface energy only influence the deformation pattern of the mineral platelet, but have little effect on its total tensile deformation.

As we all know, the deformation depends on the force. In order to understand the deformation behavior of the mineral platelet with the influence of the strain gradient and surface energy, the tensile stress in the platelet needs to be investigated. From Eq. (23a), it can be known that σ_1/σ_{max} is a function of $E_s/(E_p h)$, E_m/E_p , ϕ , ρ , β and x/L : $\sigma_1/\sigma_{max} = f(E_s/(E_p h), E_m/E_p, \phi, \rho, \beta, x/L)$. Fig. 5 shows the tensile stress in the mineral platelet P_1 along x at different β and $E_s/(E_p h)$. As shown in Fig. 5, the tensile stress in the mineral platelet has a strong size effect. For example, from Fig. 5(a), we can know that the tensile stress decreases linearly along x when there is no strain gradient and surface energy effect. With the decrease of the organic matrix thickness (namely, the gradient effect becomes strong), the stress shows a more and more obvious gradient at the end region of the platelet and becomes more and more uniform in the middle region of platelet. Interestingly, we found that the stress distribution is antisymmetric with respect to the point O. This phenomenon illustrates that although the strain gradient effect changes the state of the stress distribution, the sum of the strain produced by the stress does not change due to the antisymmetry of the stress distribution, which provides robust evidence for the unchanged total deformation of the mineral platelet shown in Fig. 4. The influence caused by the surface energy is similar to that of the strain gradient. For example, as shown in Fig. 5(b), when the surface

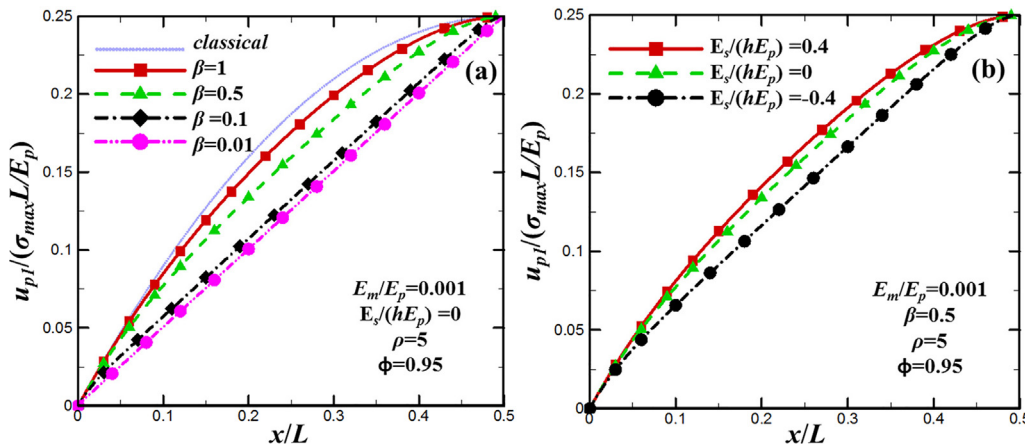


Fig. 4. The displacement of the mineral platelet P_1 along x . (a) the results at different $\beta = d/l$; (b) the results at different $E_s/(E_p h)$.

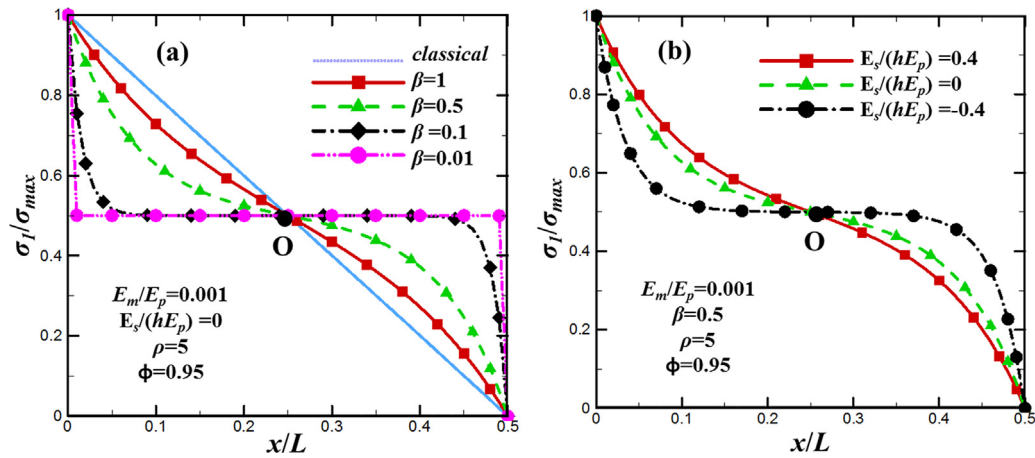


Fig. 5. The tensile stress in the mineral platelet P_1 along x . (a) The results at different $\beta = d/l$; (b) the results at different $E_s/(E_p h)$.

modulus decreases, the stress at the end region of the plate changes sharply, and the stress in the middle region of the plate is uniform. And the stress distribution is also antisymmetric with respect to the point O, which also implies that the surface energy also only influences the stress distribution but has no effect on the sum of the strain induced by the stress.

3.2. Size effect of the deformation and stress in the organic matrix

Based on Eq. (20a), it is easy to know that the normalized displacement of the organic matrix $u_m/(\sigma_{max}L/E_p)$ is a function of $E_s/(E_p h)$, E_m/E_p , ϕ , ρ , β , x/L and y/d : $u_m/(\sigma_{max}L/E_p) = f(E_s/(E_p h), E_m/E_p, \phi, \rho, \beta, x/L, y/d)$. The variation of the displacement of the organic matrix along x is consistent with that of the platelet, so it will not be analyzed again. Fig. 6 shows the displacement of the organic matrix along y at different β and $E_s/(E_p h)$. Compared to the case of the displacement of the mineral platelet along x , the influences of the strain gradient and surface energy on the displacement of the organic matrix along y is more significant. From Fig. 6(a), it can be read that the shear deformation of the organic matrix decreases with the decrease of β . Namely, the stronger the size effect caused by the strain gradient, the smaller the total shear deformation of the organic matrix. For example, in classical case ($\beta = \infty$), the displacement of the organic matrix increases with the increase of y linearly, and when y/d is 1, $u_m/(\sigma_{max}L/E_p)$ is 6.38. Along with the decrease with β , a nonlinear relationship between the displacement of the organic matrix and y is shown, and the total

shear deformation of the organic matrix becomes smaller than before. For example, the normalized total shear deformations of the organic matrix are 3.59, 1.87 and 0.41 when β are 10, 5 and 1, respectively. The reason for this is as follows: the thinner the thickness of the organic matrix, the stronger the size effect caused by the strain gradient. At this time, the nominal modulus of the organic matrix is increased and consequently, the shear deformation of the organic matrix becomes small under the same external load. In addition, the influence of the surface energy on the shear deformation of the organic matrix is similar to that of strain gradient, which is shown in Fig. 6(b). The results in Fig. 6(b) illustrate that when the surface modulus decreases, the total shear deformation of the organic decreases. For example, the normalized total shear deformations of the organic matrix are 3.09, 1.87 and 0.64 when the normalized surface moduli are 0.4, 0 and -0.4 , respectively. Combined with Fig. 4 and Fig. 6, it can be concluded that the influences of the strain gradient and the surface energy on the deformation of the organic matrix are larger than those on the platelet. Since the deformation of the staggered structure mainly derives from the shear deformation of the organic matrix, so we can say that the strain gradient and surface energy affect the deformation behavior of the staggered structure mainly by affecting that of the organic matrix.

The load determines the deformation. Therefore, in order to comprehend the shear deformation behaviors of the organic matrix, the shear stress applying on the organic matrix needs to be investigated. Based on Eq. (20b), it can be seen that the normalized shear stress

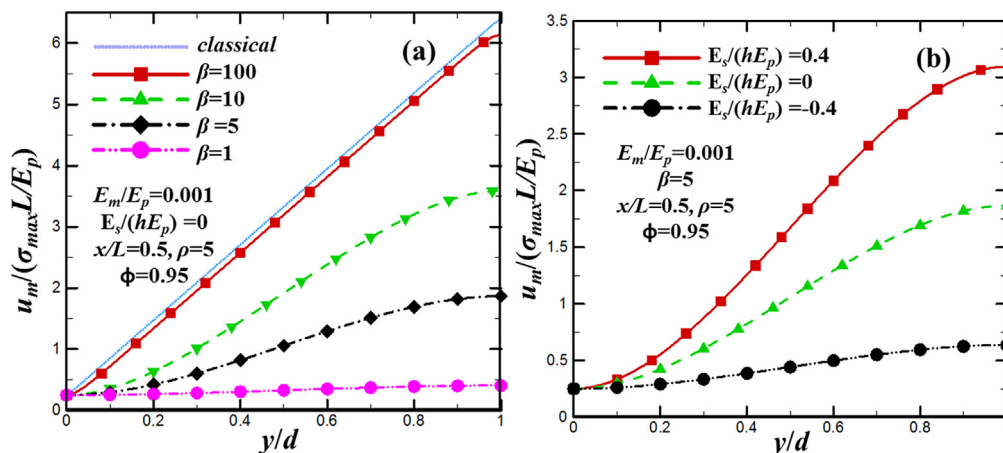


Fig. 6. The displacement of the organic matrix along y . (a) The results at different $\beta = d/l$; (b) the results at different $E_s/(E_p h)$.

t/σ_{\max} is a function of $E_s/(E_p h)$, E_m/E_p , ϕ , ρ , β and x/L : $t/\sigma_{\max} = f(E_s/(E_p h), E_m/E_p, \phi, \rho, \beta, x/L)$. Fig. 7 shows the shear stress applying on the organic matrix along x at different β and $E_s/(E_p h)$. As shown in Fig. 7, the shear stress has a strong size effect under the influence of the strain gradient and surface energy. For example, it can be known from Fig. (7a) that when β changes from 1 to 0.01, the shear stress at the middle region becomes smaller and smaller, but that at the end region increases sharply. What we want to emphasize is that although the shear stress at the end region becomes larger than before, the deformations at these regions have no significant change, which can be verified by the displacement of the platelet at $x/L = 0$ and $x/L = 0.5$. The reason for this is that the strain gradient makes the organic matrix stronger. Namely, the nominal modulus of the organic matrix becomes large. In addition, because the shear stress at the middle region is smaller and the nominal modulus is larger than before, the deformation at these regions becomes small. Therefore, with the influence of the strain gradient, the shear deformation of the organic matrix decreases significantly. The influence of the surface effect on the organic matrix is similar to that of the strain gradient, which can be seen from Fig. (7b). For example, when $E_s/(E_p h)$ changes from 0.4 to -0.4 , the shear stress in the end region decreases, which explains the reason why the shear displacement of the organic matrix decreases with the decrease of $E_s/(E_p h)$. In addition, the existence of the surface effect has a significant effect on the shear stress at the end region of the interface (e.g. $0 < x/L < 0.1$), which is enlightening to us. For example, we can change the mechanical properties of the interface to reduce the stress concentration at the end region of the interface, which is helpful to avoid interface failure.

3.3. The effective modulus of the biological staggered composites

Stiffness is usually the focus of researchers. Based on Eq. (24), it can be known that the normalized effective modulus E_c/E_p is a function of $E_s/(E_p h)$, E_m/E_p , ϕ , ρ and β : $E_c/E_p = f(E_s/(E_p h), E_m/E_p, \phi, \rho, \beta)$. Here, we focus on the influences of strain gradient and surface effect on the effective modulus. In order to investigate the influences of strain gradient and surface interface effect more clearly, we first set $E_s/(E_p h)$ as zero to investigate the influence of strain gradient alone. Fig. 8 shows the normalized effective modulus E_c/E_p as a function of E_m/E_p , ρ , and ϕ , at different β , respectively. It can be known from Fig. 8 that the normalized effective modulus increases with the increase of E_m/E_p , ρ , and ϕ at different β . The reason for this has been explained by previous researchers [8,24], so it will not be analyzed again. What we want to emphasize is that the strain gradient has significant influences on the effective modulus of the staggered structure composites. As shown in Fig. 8, under the same E_m/E_p , ρ , and ϕ , the smaller β , the larger E_c/E_p

E_p . The reason for this is as follows: when β becomes small, the strain gradient effect makes the organic matrix stronger than before. At this time, the shear deformation of the organic matrix decreases. In addition, we know that the shear deformation of the organic matrix occupies the majority of the deformation of the staggered structure composites. Therefore, under the same load, the deformation of the staggered structure composites decreases with the decrease of β . Correspondingly, the modulus of the staggered structure composites increases. In addition, it is important to note that under the influence of the strain gradient, the composites with staggered structures at microscale have an elastic modulus comparable to that of the mineral platelet.

On the basis of considering the influence of strain gradient, the surface effect is further considered by us. Fig. 9 shows the influence of surface energy on the effective modulus of the staggered structure composites with different strain gradient effects. As shown in Fig. 9, when the surface modulus decreases, the effective modulus increases. The reason for this is that the shear force applying on the organic matrix decreases with the decrease of the surface modulus. Namely, the smaller the surface modulus, the smaller the shear deformation of the organic matrix and the deformation of the staggered structure composites. Therefore, the effective modulus increases with the decrease of the surface modulus. In addition, we need to emphasize that the obviousness of the surface effect is affected by the strain gradient. As shown in Fig. 9(a), (c) and (e), when β is taken to be 1, the effective modulus of the staggered structure composites increases with the decrease of the surface modulus significantly. For example, when E_m/E_p , β , ρ and ϕ are respectively 0.001, 1, 5 and 0.95, the effective moduli are 0.49, 0.58 and 0.75 as $E_s/(hE_p)$ changes from -0.4 to 0.4. The difference in effective moduli can be up to $\sim 53\%$. However, when β is taken to be 0.01, the effective modulus of the staggered structure composites increases with the decrease of the surface modulus slightly. For example, when E_m/E_p , β , ρ and ϕ are respectively 0.001, 0.01, 5 and 0.95, the effective moduli are 0.9426, 0.9445 and 0.9475 as $E_s/(hE_p)$ changes from -0.4 to 0.4. The difference in effective moduli is $\sim 0.52\%$. The above results give us an inspiration. That is, with the aid of strain gradients and surface interface effects, composite materials with structural design from the nanoscale will have outstanding mechanical properties at the macroscopic scale.

4. Model validation

In this section, the effective moduli predicted by our trans-scale shear-lag model are compared with the experiments to verify the effectiveness of the model. In our model, there are two key parameters that need to be decided. They are the characteristic length scale of the

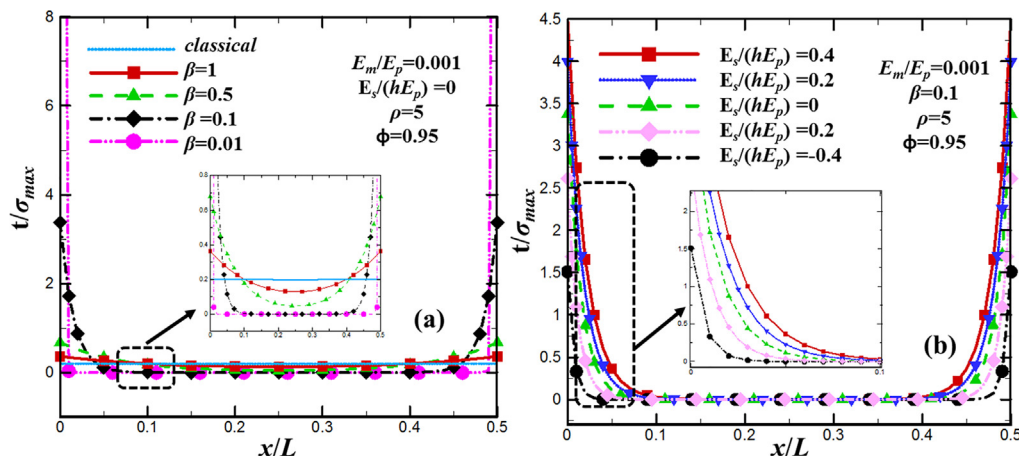


Fig. 7. The shear force applying on the organic matrix along x . (a) The results at different $\beta = d/l$; (b) the results at different $E_s/(E_p h)$.

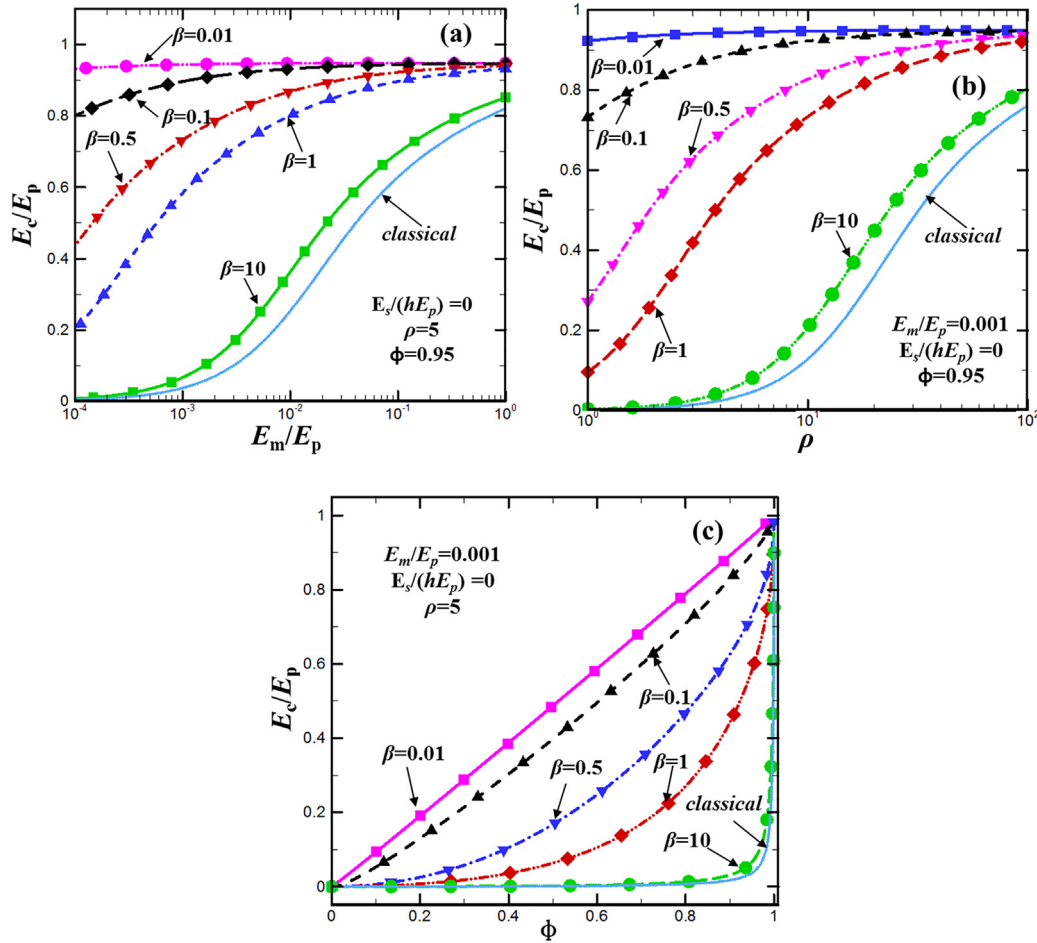


Fig. 8. The effective moduli of the staggered structure composite under the influence of the strain gradient. (a) The relationship between E_c/E_p and E_m/E_p ; (b) the relationship between E_c/E_p and ρ ; (c) the relationship between E_c/E_p and ϕ .

organic matrix, l , and the surface Young's modulus, E_s . Their values have been studied by previous researchers. For example, based on an elegant micromechanical model, Nikolov et al. estimated that the non-local length scale of the rubbers is in the neighborhood of 5 nm [44]; Lam et al. suggested that materials like epoxy have a length scale of 10 μm based on experiments and strain gradient theory [45]. The characteristic scale of polymer has a large span (5 nm \sim 10 μm). As we all know that the organic matrix belongs to polymer compounds. Therefore, referring to the characteristic length of polymers, we take the characteristic length of the organic matrix as 0.1 μm . In addition, due to lack of the work about the surface modulus of the biological materials, we can estimate it based on the studies about the ceramic interface or metal. Following the works [46,47], taking E_s as $-100 \sim 100$ N/m is reasonable, which is also adopted by the previous researcher [34]. According to the references, we take E_s as 50 N/m in the following results. The geometry and mechanical parameters used in calculations are selected from previous researches, which are list in Table 1. It should be noted that due to lack of the exact modulus of the platelets and organic matrix of pintada and red abalone, the previous researcher estimated $E_p = 94$ GPa and $E_m = 0.1$ GPa based on Voigt model [24], which is also adopted by us. For the selection of the parameters of the bone, we adopt them based on references [6,7].

The predicted effective moduli by previous models and our trans-scale shear-lag model are compared with the experiment results, which are shown in Table 2. Here, we need to explain that the longitudinal modulus of collagen fibrils in bone is related to humidity [50]. Previous researches have shown that the lower the relative humidity, the

higher the modulus of the collagen fibrils in bone. Therefore, according to previous researches [6,7,48,49], the modulus of the collagen fibrils in bone is usually between 10 GPa and 20 GPa. First of all, from Tab. 2, we can know that the effective moduli predicted by our model is closer to that of the experiment than other models, which verifies the effectiveness of our model. Secondly, as you know, the work about the characteristic length scale of the organic matrix is none. In our paper, referring to the characteristic length of polymers (5 nm \sim 10 μm), the characteristic length scale of the organic matrix is taken to be 0.1 μm , which leads to a slightly high predicted result. But if the characteristic length scale of the organic matrix is taken as 0.01 μm , then there will be gratifying results. For example, the effective moduli predicted by our model with $l = 0.01$ μm for pintada, abalone and bone are 66.59 GPa, 64.94 GPa and 15.04 GPa, respectively. At this time, it can be found that our model can well predict the effective modulus of shell and bone. We do not know the exact value of the characteristic length scale of the organic matrix l . What we want to express here is that our model is more reasonable than other models in predicting the effective modulus of the biological staggered composites.

5. Conclusions

In order to understand the relationship between the micro-nano staggered structure of the biological composites and their excellent mechanical properties, a trans-scale shear-lag model is established based on the strain gradient theory and Gurtin-Murdoch model in this

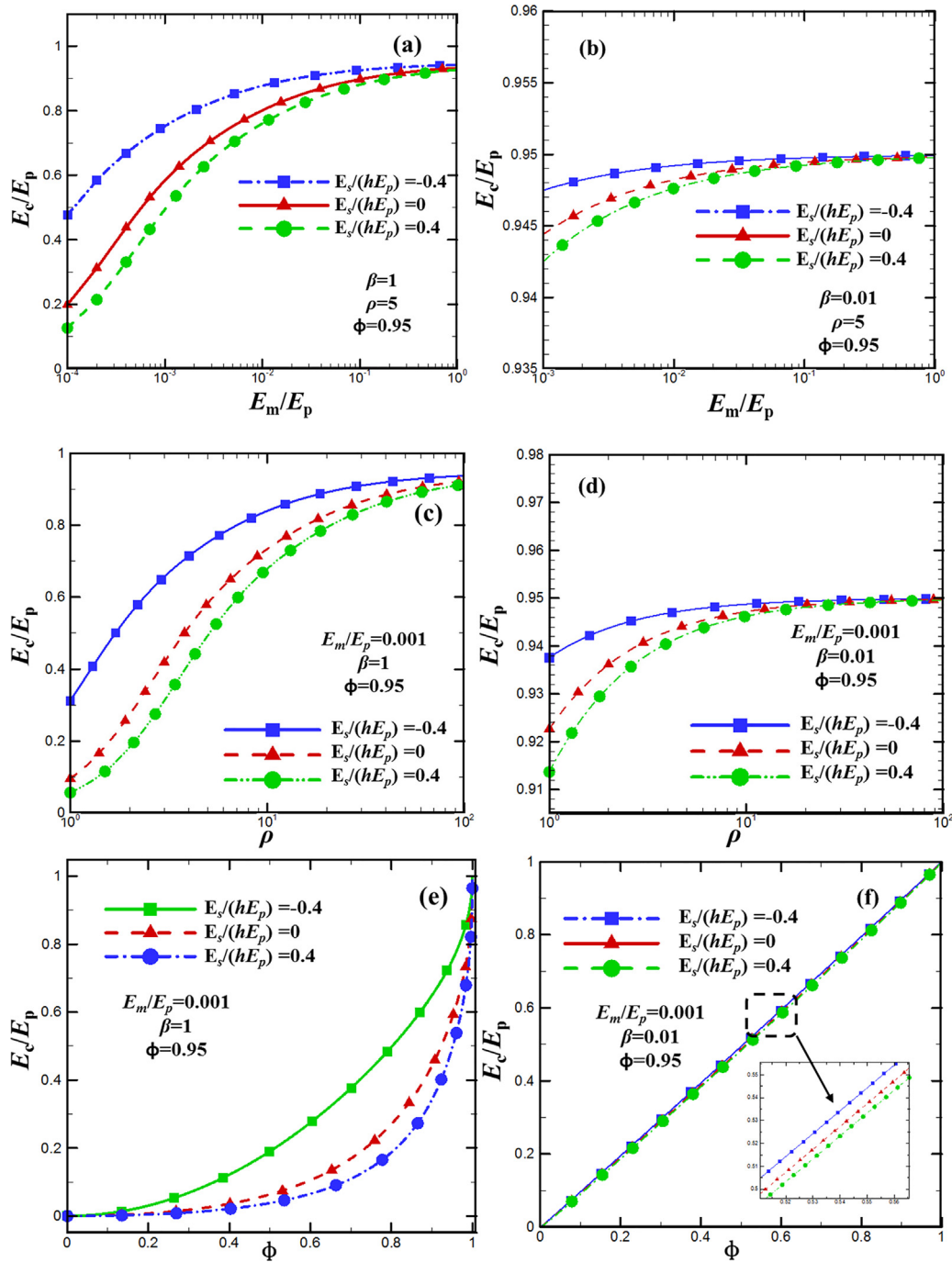


Fig. 9. The effective moduli of the staggered structure composite under the influences of strain gradient and surface effect. (a) and (b) are the relationship between E_c/E_p and E_m/E_p , β is 1 in (a) and 0.01 in (b); (c) and (d) are the relationship between E_c/E_p and ρ , β is 1 in (c) and 0.01 in (d); (e) and (f) are the relationship between E_c/E_p and ϕ , β is 1 in (e) and 0.01 in (f).

Table 1
The geometry and mechanical parameters selected from experiments.

Samples	L(μm)	h(μm)	d(nm)	E_p (GPa)	E_m (GPa)	$\rho = L/l$	$\phi = h/(h + d)$
Shell/Pinctada [4]	4	0.4	15	94	0.1	10	96.4%
Shell/Red abalone [43]	6.5	0.55	20	94	0.1	11.8	96.5%
Bone/Collagen fibrils [6,7]	0.05	0.002	3	50	0.05	25	40.0%

paper. By theoretical analysis, two dimensionless numbers d/l and $E_s/(hE_p)$ are proposed to characterize the size effects caused by the thickness of the organic matrix and the platelet, respectively. Following

that, the deformations and stress distribution are investigated based on our model systematically. The results reveal that under the influence of the strain gradient and surface energy, the deformations and

Table 2

The effective moduli (GPa) predicted by previous models and our model compared with the experiment results [4,43,48,49].

	SL	BW	TSC	Dong	Present model	Experiments
Shell/Pinctada	16.30	16.31	17.32	17.34	87.41	70 ± 11 [4]
Shell/Red abalone	21.28	21.29	23.04	23.06	87.17	69 ± 7 [43]
Bone/Collagen fibrils	0.66	0.67	0.67	0.69	19.36	10–20 [6,7,48,49]

stress distributions have strong size effects. For the mineral platelet, the strain gradient and the surface energy only have influences on the local deformations and stress distributions but have no effects on the total tensile deformation of the platelet. For example, the total normalized displacement of the platelet has no change under the influences of the strain gradient and the surface energy. However, as regards to the organic matrix, the influences of the strain gradient and the surface energy on the local deformations, stress distributions and total shear deformation are significant. For example, the characteristics of the shear stress applied on the organic matrix changed significantly under the influences of the strain gradient and surface energy. And the stronger the strain gradient effect or the surface effect, the greater their influences on the deformation of the organic matrix. Because the deformation of the organic matrix occupies the majority of the deformation of the staggered structure composites, it can be concluded that the strain gradient and the surface energy influence the deformation behaviors of the staggered structure composites mainly by influencing those of the organic matrix. Due to the strong interest of researchers on the stiffness, the effective modulus of the biological staggered composites is also analyzed in detail. We find that the effective modulus of the staggered structure composites also has a strong size effect, which implies that the influences of the strain gradient and the surface energy are important and cannot be neglected. In addition, in order to verify the effectiveness of our model, the effective moduli predicted by our model are compared with the experimental results. The results illustrate that the trans-scale model in this paper can better predict the effective modulus of the biological staggered composites. Our model provides a chance to glimpse how the micro-nano staggered structures of the biological composites determine its macroscopic mechanical behavior for the first time, which provides theoretical guidance for the design of the high-performance bionic composite materials.

CRediT authorship contribution statement

Yanwei Liu: Conceptualization, Formal analysis, Methodology, Writing - original draft. **Hansong Ma:** Methodology, Writing - review & editing. **Hao Long:** Formal analysis, Writing - review & editing. **Yue-guang Wei:** Conceptualization, Funding acquisition, Resources, Supervision, Writing - review & editing.

Declaration of Competing Interest

The authors declare that they have no known competing financial interests or personal relationships that could have appeared to influence the work reported in this paper.

Acknowledgments

This work is supported by the National Natural Science Foundation of China under grants no. 11890681, 11672301, 11572329, 11521202, and 11432014.

References

[1] Kamat S, Su X, Ballarini R, Heuer AH. Structural basis for the fracture toughness of the shell of the conch *Strombus gigas*. *Nature* 2000;405(6790):1036–40.

[2] Menig R, Meyers MH, Meyers MA, Vecchio KS. Quasi-static and dynamic mechanical response of *Haliotis rufescens* (abalone) shells. *Acta Mater* 2000;48(9):2383–98.

[3] Menig R, Meyers MH, Meyers MA, Vecchio KS. Quasi-static and dynamic mechanical response of *Strombus gigas* (conch) shells. *Mater Sci Eng, A* 2001;297(1–2):203–11.

[4] Jackson AP, Vincent JFV, Turner RM. The Mechanical Design of Nacre, Proceedings of the Royal Society of London. Series B, Biological sciences 234 (1277) (1988) 415–440.

[5] Wegst UGK, Ashby MF. The mechanical efficiency of natural materials. *Phil Mag* 2004;84(21):2167–86.

[6] Norman TL, Vashishth D, Burr DB. Fracture toughness of human bone under tension. *J Biomech* 1995;28(3):309–20.

[7] Jager I, Fratzl P. Mineralized collagen fibrils: A mechanical model with a staggered arrangement of mineral particles. *Biophys J* 2000;79(4):1737–46.

[8] Ji B, Gao H. Mechanical properties of nanostructure of biological materials. *J Mech Phys Solids* 2004;52(9):1963–90.

[9] Dunlop JWC, Fratzl P. Biological Composites, in: Clarke DR, Ruhle M, Zok F. (Eds.), *Annual Review of Materials Research*, Vol 402010, pp. 1–24.

[10] Sun J, Bhushan B. Hierarchical structure and mechanical properties of nacre: a review. *RSC Adv* 2012;2(20):7617–32.

[11] Currey JD. Mechanical properties of mother of pearl in tension. Proceedings of the Royal Society Series B-Biological Sciences 1977;196(1125):443–+.

[12] Weiner S, Wagner HD. The material bone: Structure mechanical function relations. *Annu Rev Mater. Sci.* 1998;28(1):271–98.

[13] Barthelat F. Biomimetics for next generation materials. *Philosophical Transactions of the Royal Society a-Mathematical Physical and Engineering Sciences* 2007;365(1861):2907–19.

[14] Jackson AP, Vincent JFV, Briggs D, Crick RA, Davies SF, Hearn MJ, et al. Application of surface analytical techniques to the study of fracture surfaces of mother-of-pearl. *J Mater Sci Lett* 1986;5(10):975–8.

[15] Dai Y, Mai Y-W, Ji X. Predictions of stiffness and strength of nylon 6/MMT nanocomposites with an improved staggered model. *Composites Part B-Engineering* 2008;39(6):1062–8.

[16] Zhang ZQ, Liu B, Huang Y, Hwang KC, Gao H. Mechanical properties of unidirectional nanocomposites with non-uniformly or randomly staggered platelet distribution. *J Mech Phys Solids* 2010;58(10):1646–60.

[17] Lei HF, Zhang ZQ, Liu B. Effect of fiber arrangement on mechanical properties of short fiber reinforced composites. *Compos Sci Technol* 2012;72(4):506–14.

[18] Zuo S, Wei Y. Effective elastic modulus of bone-like hierarchical materials. *AcMSS* 2007;20(3):198–205.

[19] Bar-On B, Wagner HD. Mechanical model for staggered bio-structure. *J Mech Phys Solids* 2011;59(9):1685–701.

[20] Barthelat F, Tang H, Zavattieri PD, Li CM, Espinosa HD. On the mechanics of mother-of-pearl: A key feature in the material hierarchical structure. *J Mech Phys Solids* 2007;55(2):306–37.

[21] Gao H. Application of fracture mechanics concepts to hierarchical biomechanics of bone and bone-like materials. *IJFr* 2006;138(1–4):101–37.

[22] Gao X-L, Zhang GY. A microstructure-and surface energy-dependent third-order shear deformation beam model. *Z Angew Math Phys* 2015;66(4):1871–94.

[23] Liu Y, Ma H, Wei Y, Chen P. Size effect investigation of indentation response of stiff film/compliant substrate composite structure. *IJSS* 2020;193–194:106–16.

[24] Ma H, Wei Y, Song J, Liang L. Mechanical behavior and size effect of the staggered bio-structure materials. *Mech Mater* 2018;126:47–56.

[25] Mindlin RD. Micro-structure in linear elasticity. *ArRMA* 1964;16(1):51–78.

[26] Papargyri-Beskou S, Beskos DE. Static, stability and dynamic analysis of gradient elastic flexural Kirchhoff plates. *Arch Appl Mech* 2008;78(8):625–35.

[27] Papargyri-Beskou S, Giannakopoulos AE, Beskos DE. Variational analysis of gradient elastic flexural plates under static loading. *IJSS* 2010;47(20):2755–66.

[28] Gurtin ME, Ian Murdoch A. A continuum theory of elastic material surfaces. *ArRMA* 1975;57(4):291–323.

[29] Wang J, Huang Z, Duan H, Yu S, Feng X, Wang G, et al. Surface stress effect in mechanics of nanostructured materials. *AcMSS* 2011;24(1):52–82.

[30] He J, Lilley CM. Surface effect on the elastic behavior of static bending nanowires. *Nano Lett* 2008;8(7):1798–802.

[31] Wang G-F, Feng X-Q. Effects of surface elasticity and residual surface tension on the natural frequency of microbeams. *Appl Phys Lett* 2007;90(23):231904. <https://doi.org/10.1063/1.2746950>.

[32] Wang Z-Q, Zhao Y-P, Huang Z-P. The effects of surface tension on the elastic properties of nano structures. *IJES* 2010;48(2):140–50.

[33] Chen C, Shi Y, Zhang YS, Zhu J, Yan Y. Size dependence of Young's modulus in ZnO nanowires. *Phys Rev Lett* 2006;96(7):075505.

[34] Dong L, Chao C, Yan P. Effective modulus of biological staggered nanocomposites with interface stress effect. *Compos B Eng* 2019;166:701–9.

- [35] Wei Y, Hutchinson JW. Steady-state crack growth and work of fracture for solids characterized by strain gradient plasticity. *J Mech Phys Solids* 1997;45(8):1253–73.
- [36] Ma H, Hu G, Wei Y, Liang L. Inclusion problem in second gradient elasticity. *IJES* 2018;132:60–78.
- [37] Placidi L, Andraus U, Corte AD, Lekszycki T. Gedanken experiments for the determination of two-dimensional linear second gradient elasticity coefficients. *Z Angew Math Phys* 2015;66(6):3699–725.
- [38] Placidi L, Andraus U, Giorgio I. Identification of two-dimensional pantographic structure via a linear D4 orthotropic second gradient elastic model. *J Eng Math* 2017;103(1):1–21.
- [39] Duan HL, Wang J, Huang ZP, Karihaloo BL. Size-dependent effective elastic constants of solids containing nano-inhomogeneities with interface stress. *J Mech Phys Solids* 2005;53(7):1574–96.
- [40] Rosi G, Placidi L, Nguyen V-H, Naili S. Wave propagation across a finite heterogeneous interphase modeled as an interface with material properties. *MeReC* 2017;84:43–8.
- [41] Povstenko YZ. Theoretical investigation of phenomena caused by heterogeneous surface tension in solids. *J Mech Phys Solids* 1993;41(9):1499–514.
- [42] Song J, Fan C, Ma H, Wei Y. Hierarchical structure observation and nanoindentation size effect characterization for a limnetic shell. *AcMSn* 2015;31(3):364–72.
- [43] Wang RZ, Suo Z, Evans AG, Yao N, Aksay IA. Deformation mechanisms in nacre. *J Mater Res* 2001;16(9):2485–93.
- [44] Nikolov S, Han C-S, Raabe D. On the origin of size effects in small-strain elasticity of solid polymers. *IJSS* 2007;44(5):1582–92.
- [45] Lam DCC, Yang F, Chong ACM, Wang J, Tong P. Experiments and theory in strain gradient elasticity. *J Mech Phys Solids* 2003;51(8):1477–508.
- [46] Mi C, Jun S, Kouris DA, Kim SY. Atomistic calculations of interface elastic properties in noncoherent metallic bilayers. *PhRvB* 2008;77(7). <https://doi.org/10.1103/PhysRevB.77.075425>.
- [47] Pahlevani L, Shodja HM. Surface and interface effects on torsion of eccentrically two-phase fcc circular nanorods: determination of the surface/interface elastic properties via an atomistic approach. *Journal of Applied Mechanics-Transactions of the Asme* 2011;78(1).
- [48] Harley R, James D, Miller A, White JW. Phonons and elastic-moduli of collagen and muscle. *Nature* 1977;267(5608):285–7.
- [49] Eppell SJ, Smith BN, Kahn H, Ballarini R. Nano measurements with micro-devices: mechanical properties of hydrated collagen fibrils. *J R Soc Interface* 2006;3(6):117–21.
- [50] Wenger MPE, Bozec L, Horton MA, Mesquida P. Mechanical properties of collagen fibrils. *Biophys J* 2007;93(4):1255–63.